A Large-Eddy Simulation Of Turbulent Flow Over A Backward Facing Step

James R. DeBonis*
NASA Glenn Research Center, Cleveland, Ohio 44135

Large-eddy simulation (LES) was used to study the turbulent flow over a backward facing step. The simulations examine the details of the turbulent flow's separated and reattaching regions created by the step geometry. An explicit high-order of accuracy/high resolution finite-difference computational fluid dynamics solver was used for both LES and Reynolds-averaged Navier-Stokes (RANS) simulations. The experimental data from the backward facing step experiment of Driver and Seegmiller was used for comparison. Data presented are derived from a RANS simulation using the Spalart-Allmaras turbulence model and LES simulations using the implict LES assumption on three different grids of varying resolution. The RANS solution agrees with past work. It does an adequate job of predicting the flowfield and reattachment point, but misses details such as the strength of the recirculating region and magnitudes of the Reynolds stresses. The synthetic eddy method was used to provide a turbulent inflow to the quasi-2D LES domains. For the LES, the coarse grid was of insufficient resolution and under-predicted the skin friction coefficient and over-predicted the normal stresses. The finer grid LES results accurately predict the skin friction coefficient and provide more accurate Reynolds stresses. Triple product velocity correlations are also computed from the LES and the finer grid results did a good job predicting the magnitudes of the curves and the shapes were reasonably represented. It is recommended that future work include investigating the turbulent inflow domain length, width of the quasi-2D domain, and additional grid refinement.

Nomenclature

i, j, k	grid indices
p	pressure
t	time
u_i	velocity vector, $u_1 = u$, $u_2 = v$, $u_3 = w$
$< u_i u_j >$	Reynolds stress tensor
$< u_i u_j u_k >$	Triple product correlation tensor
x, y, z	cartesian coordinates
C_f	skin friction coefficient
H	step height (reference length)
L	length of computational domain
M_{ref}	reference Mach number
Re_H	Reynolds number based on step height
T	temperature
U_{ref}	reference velocity
Δx, Δy, Δz	grid spacing in x-, y-, and z-directions
δ	boundary layer thickness
τ	characteristic time

subscripts

0	stagnation condition

*Aerospace Engineer, Inlet & Nozzle Branch, james.r.debonis@nasa.gov, Associate Fellow AIAA

avg	average quantity
max	maximum

superscripts

+	distance in wall units

I. Introduction

Despite decades of effort, the accurate prediction of turbulent flow separation remains one of the most important challenges for for computational fluid dynamics (CFD).[1] Flow separation affects the efficiency and operability of countless fluid dynamic systems. Some examples include aircraft stall, high-lift systems, subsonic inlets at high angle-of-attack or crosswind, supersonic inlet unstart and compressor stall. The lack of accurate prediction methods requires the developers to undertake expensive model-scale and flight tests, and build in additional margin to the design - sacrificing efficiency. Up to now, the primary tool used to predict these flow has been Reynolds-averaged Navier-Stokes (RANS) codes. They have proven effective for attached flows but fail where separation is a dominant feature. Improvements in RANS turbulence models are no longer expected to be able to enable accurate prediction of such flows. Two of the most widely used linear eddy viscosity models, Spalart-Allmaras[2] and the Shear Stress Transport model[3] are over 25 years old. More advanced models such as explicit algebraic stress models and full Reynolds stress models have not consistently shown a benefit over the older linear models. Scale resolving simulations, large-eddy simulation (LES) and direct numerical simulation, have demonstrated the ability to very accurately predict turbulent flow phenomena, albeit at a much higher cost. But, we are at a point where computing power is sufficient for LES to become a more widely used prediction tool for separated flow.

Flow separation is a complex phenomenon involving the interaction of a turbulent boundary layer with an adverse pressure gradient. The flow separates, or leaves the surface, at the separation point and reattaches to the surface further downstream. Between these two points is a complex flowfield consisting of a recirculating region connected by a shear layer above. The separation and reattachment points are coupled to each other further complicating the physics. The backward facing step flow is an attempt to simplify the flow by fixing the separation point and removing the strong adverse pressure gradient. The recirculating flow, shear layer and reattachment process remain. The backward facing step has become a canonical flow in the investigation of separated flows.

The National Aeronautics and Space Administration's (NASA's) Transformational Tools and Technologies project (TTT) is developing scale resolving simulation based methods, measurement techniques and resulting data to impact future aerospace vehicles and technologies. An important focus of TTT is improving our computational fluid dynamics capabilities. To this end, a detailed study of a backward facing step using both LES and RANS methods has been undertaken here. The experimental configuration and data from Driver and Seegmiller[4] is used. The Wave Resolving Large Eddy Simulation (WRLES) code[5] is used to solve both the Reynolds-averaged and Favre-filtered forms of the Navier-Stokes equations. The Spalart-Allmaras turbulence model is used to close the RANS equations. The implicit sub-grid scale modeling technique is used for the LES. The goals of this study are to further mature our LES techniques, and to improve our understanding of the backward facing step flow.

II. Backward Facing Step Experiment

Driver and Seegmiller's backward facing step experiment[4] is a widely used test case for turbulence model developers and testers. It is included on on the NASA Langley Turbulence Modeling Resource webpage,[6] the NPARC Alliance Verification and Validation Archive,[7] and the European Research Community On Flow Turbulence and Combustion Classic Collection Database.[8]

The experimental configuration consists of an enclosed wind tunnel having a rectangular cross-section with a backward facing step to induce flow separation (figure 1). The flow is incompressible and is nominally two-dimensional due to the large width of the tunnel compared to the step height. The step height, H is 1.27 cm (0.5 inches). The height of the tunnel upstream of the step is $8H$, and the width is $12H$. The data consists primarily of laser doppler velocimetry measurements and contains mean velocities, Reynolds stresses and triple product correlations. Skin friction and pressure coefficients along the tunnel wall are also reported.

The flow conditions at a reference station $4H$ before the step are reported in table 1.

Table 1: Flow conditions at $x/H = -4$, note: $H = 1.27$ cm

Quantity	value	units
U_{ref}	44.04	m/s
M_{ref}	0.128	
p_0	101.35	kPa
T_0	297	K
δ	$1.5H$	
Re_H	36,000	

III. Numerical Simulations

Both the RANS simulations and LES were performed using the same CFD code. The RANS simulation was performed to provide a baseline CFD solution for comparison. It was also used a fast means to determine the correct downstream static pressure for the LES solution, and to provide data for the inflow boundary conditions of the LES. The LES data and improved methodology serves as the primary product of this work.

A. Flow Solver - WRLES

The code used in this study, WRLES (Wave Resolving Large-Eddy Simulation),[5] is a special purpose LES code that uses high-resolution temporal and spatial discretization schemes to accurately simulate the convection of turbulent structures. The code solves the compressible Navier-Stokes equations on structured meshes using generalized curvilinear coordinates. It is written entirely in Fortran 90 and utilizes both Message Passing Interface (MPI) libraries[9] and OpenMP compiler directives[10] for parallelization. WRLES has been previously used and validated for jet flows.[11–15] This is the first detailed study of wall-bounded flows using WRLES.

WRLES employs explicit finite-difference methods to solve the equations. Central-differencing operators up to 12th-order accuracy are implemented for the spatial discretization. Both standard central-difference stencils and dispersion relation preserving (DRP) stencils from Bogey and Bailley,[16] and Tam and Shen[17] are available. Skewed high-order stencils are used near the solid walls to maintain high-resolution. Near the other boundaries, central difference stencils of reducing order are used to help eliminate reflecting waves. Solution filtering is used to provide stability with minimal dissipation. Filters developed by Kennedy and Carpenter[18] are used for the standard central difference operators. For the DRP schemes, filters tailored to dispersion properties of the individual DRP schemes were implemented.

Time advancement is performed using 2N-storage Runge-Kutta schemes. There are numerous options available in the code.

B. RANS Solutions

The RANS solution serves two primary purposes; 1) to serve as the standard for comparison of the LES solutions, and 2) to provide inflow conditions to the LES.

1. RANS Methodology

The RANS simulation is a two-dimensional simulation. The effect of the wind tunnel sidewalls is ignored. The long duct upstream of the backward facing step is modeled, in order to develop the correct boundary layer properties at the reference station upstream of the step.

The Spalart-Allmaras (SA) turbulence model was recently added to the WRLES code and is used for the RANS simulations. The addition of the RANS model caused stability problems for the low-dissipation high-order code. The standard 10-order central differencing in conjunction with the Kennedy and Carpenter 12th-order filter were used, as they provided a more stable solution than the DRP schemes.

Carpenter and Kennedy's 4-stage 3rd-order Runge-Kutta scheme was used for time advancement. Local time stepping was used to speed convergence. Here, a CFL number was specified and used to compute a time step for each grid point. The time step was smoothed using a 2nd-order filter to aid stability. The solution at each point was then advanced according to its own time step, until a steady state was reached.

2. RANS Grids

The WRLES code is a three-dimensional code. In order to obtain a two-dimensional solution, a grid consisting of 13 uniformly spaced planes in the z-direction was used. This accommodates the 13-point finite difference and filtering stencils in the 3rd direction; the maximum stencil width. To generate a turbulent boundary layer that matches the experimental conditions at the reference plane ($x/H = -4$), the inflow of the domain starts $118H$ upstream of the step ($x/H = 0$) and the viscous walls start at $110H$ upstream of the step. The domain extends $50H$ downstream of the step, with the majority of the grid points concentrated in the first 10 step heights. The spacing of the first grid point off of the viscous walls was constant throughout the grid and was chosen to ensure a $y^+ = 1$ at the reference plane. A total of 613,561 grid points were used in this calculation.

3. RANS Boundary Conditions

Total pressure and total temperature were specified at the inflow plane. Static pressure was specified at the exit plane downstream. The exact value of the static pressure was modified in order to obtain the correct velocity at the reference plane upstream of the step. The viscous walls were considered to be adiabatic. Periodic boundary conditions were imposed on the sidewall boundaries to impose a zero gradient condition in this direction to facilitate 2D flow.

C. LES Solutions

1. LES Methodology

For this work, the 11-point dispersion relation preserving (DRP) scheme, and matching solution filter of Bogey and Bailley were used for the spatial discretization.[16] Near the viscous wall boundaries, Berland's boundary stencils, designed to preserve the DRP properties of the scheme, were used.[19] Near the other boundaries central difference and filter stencils of reducing order were employed to enhance stability. For the LES, implicit sub-grid scale modeling was employed. This technique assumes that the numerical dissipation inherent in the solution serves to dissipate the energy of the smallest turbulent scales. The suitability of WRLES for implicit LES was demonstrated in reference 14.

Berland's 6-stage, 4th-order Runge-Kutta scheme was employed.[20] It was found that this scheme provided an efficiency benefit by enabling larger time-steps for the computational work done. A global time step was used to advance the solution. During the initial stages of the solution, a stable CFL number was specified and a time step was computed at each grid point. The smallest time step in the domain was then used to advance the solution everywhere. This allows the time step to varying from iteration to iteration. Once the flow was established and the start-up transients had cleared the domain, a constant time-step was used to advance the solution.

2. LES Grids

To reduce the computational cost of the LES solution, the domain upstream of the step was truncated and boundary conditions were used to simulate the turbulent flow there (see below). The domain extends downstream of the step for the same $50H$ as the RANS grid. The grid spacing is stretched near the outflow plane to damp pressure waves to avoid reflection back into the domain. The experiment used a wide tunnel ($12H$) to provide two-dimensional flow near the center of the tunnel. To simulate this quasi-2D flow, a domain width of $4H$ was used and periodic boundaries were imposed on the sides. This simulates the middle third of the experimental tunnel, assuming that the flow was two-dimensional in this region.

Three different grids were used for the present results. The first grid was the coarsest. The inflow plane was placed at $x/H = -8$. The grid spacings in the boundary layer upstream of the step were found in post-processing to be: $\Delta x^+ = 30$, $\Delta y^+ = 0.75$ and $\Delta z^+ = 23$. Note that all wall units reported are based

on the wall shear stress at the reference plane. As will be discussed later, the solution on this grid underpredicts the value of the wall shear stress, causing the grid spacings expressed in wall units to be smaller than intended. The intended grid spacing for the coarse grid were: $\Delta x^+ = 40$, $\Delta y^+ = 1$ and $\Delta z^+ = 30$. Downstream of the step ($x/H = 0$) the grid gradually stretches to $x/H = 12$. Beyond that point, the grid stretches more rapidly to damp any waves reflecting from the outflow plane; results here are not considered accurate. The second grid replicated the first grid's topology, but had finer grid spacings. The grid spacings upstream of the step were : $\Delta x^+ = 22$, $\Delta y^+ = 1$ and $\Delta z^+ = 17$. The third grid extended the inflow plane further upstream to $x/H = -12$. It used the same grid spacings upstream of the step. Downstream of the step, the grid stretched more gradually and this region was extended to $x/H = 15$. A summary of the grid parameters can be found in table 2. Because grid resolution is critical for scale-resolving methods, an attempt to quantify the grid structure beyond the typical number of grid points has been made here. Plots of the axial and vertical grid spacings are shown in figure 3. Note that the Δz^+ spacing is given above and is constant throughout the domain. The hope is that others attempting similar analyses may find these useful for comparison.

3. LES Boundary Conditions

On the inflow plane, the mean flow quantities (density, velocities, temperature and Reynolds stress tensor) from the RANS solution are imposed in the boundary layers and fluctuating components to these quantities are generated using the synthetic eddy method (SEM) of Jarrin.[21] The SEM provides fluctuating velocities that will replicate the Reynolds stress profiles provided. The basic SEM was modified to incorporate fluctuations in the thermodynamic variables using the method of Touber and Sandham.[22] This modification provides time varying density and temperature corresponding to the velocity fluctuations, and reduces the large pressure waves created by the baseline SEM, which destabilized early simulation attempts. It is possible to apply the SEM across the entire inflow domain, but this creates two problems: 1) the subsonic inflow boundary would be ill-posed everywhere due to the complete specification of all variables, 2) the computational cost of such a large SEM boundary would be significant. Therefore, outside of the boundary layers a subsonic inflow boundary condition where total pressure and temperature are held constant is used to alleviate these concerns. In addition to the inflow profiles SEM also requires a convective velocity and length scale. The convective velocity specified was 24 m/s and the length scale was 0.3 cm (approximately 1/6th of the boundary layer thickness0).

To create a quasi-2D solution, periodic conditions are imposed on the span-wise boundaries. No-slip adiabatic conditions are imposed on the solid walls. The outflow boundary imposes a constant static pressure for subsonic flow. This static pressure was initially set to the value used in the RANS solution, but had to be adjusted to provide the correct flow conditions at the reference plane at $x/H = -4$.

Table 2: Computational Grid Sizes

		Block 1 Upstream of Step			Block 2 Downstream of Step			
Case	inflow (x/H)	i_{max}	j_{max}	k_{max}	i_{max}	j_{max}	k_{max}	Total Pts.
RANS	-110	225	101	13	152	161	13	613,561
LES Grid 1	-8	277	141	185	386	241	185	24,435,355
LES Grid 2	-8	501	301	331	570	441	331	133,118,601
LES Grid 3	-12	751	301	331	850	441	331	198,898,231

IV. Results

The RANS solution was advanced using a local time step which was computed based on a specified CFL number. The back pressure was iteratively adjusted until the correct velocity at the reference plane was achieved. Then, the solution was monitored, and convergence was achieved when skin friction, pressure coefficient, mean velocities and turbulent quantities were unchanged between 10,000 iteration intervals.

Reynolds stresses were obtained from the RANS variables using the method described in reference 23. It is important to note that only the shear stress is used in the RANS calculation. The normal stresses reported from this method are approximate.

The LES solutions were started from the final RANS solution using the same downstream pressure. It was found that additional adjustment of the back-pressure was required to provide the same conditions at the reference station upstream of the step, indicating that the total pressure losses in the two solutions differed. An instantaneous solution from the grid 3 LES is shown in figure 2 to illustrate to complex nature of the flow. The image focuses on the lower boundary layer upstream of the step, and the separated region downstream of the step. Iso-contours of q-criterion, representing turbulent structures, are plotted. The coloring represents the axial velocity. A vast array of structures, ranging in size from the very small near wall eddies to the large hairpin vortices, are seen. Once the correct inflow conditions were achieved , the solution was time averaged. The averaging time is reported based on a characteristic time computed using the reference velocity and a reference length, $\tau = L_{ref}/U_{ref}$. Characteristic times based on the step height, H, and the length of the computational domain, L, are reported. The averaging times for each LES solution is given in table 3. Advantage was taken of the fact that the turbulence was homogenous in the span-wise direction and the time-averaged three-dimensional solution was then averaged over the span to produce a final two-dimensional time-averaged solution.

Table 3: Time required for converged time averages.

Grid	t_{avg} (s)	t_{avg}/τ_H	t_{avg}/τ_L
1	$2.39 \cdot 10^{-1}$	829	14.3
2	$9.87 \cdot 10^{-2}$	341	5.88
3	$2.11 \cdot 10^{-1}$	732	11.8

A. Velocity Contours

Time averaged axial velocity contours from the LES solution on the finest grid are shown in figure 4. Upstream of the step, a uniform core flow is bounded by turbulent boundary layers on the upper and lower walls approximately 1.5 step heights thick. Behind the step, a large low-speed region persists (figure 4b). This region is dominated by a large recirculating/separated region connected to the core flow by a shear layer. Streamlines reveal that in addition to the large separation, a smaller counter-rotating vortex exists in the corner (figure 4c).

B. Skin Friction

Skin friction coefficient is plotted in figure 5. The high-order numerics used in this study created an oscillatory or ringing behavior in the immediate vicinity of the step. It does not appear to have any adverse effect on the overall solution. The RANS solution using the Spalart-Allmaras model starts $110H$ upstream of the step. This length was chosen so that the skin friction at the reference station ($x/H = -4$) matches the experimental value. In the separated region the SA model produces too strong a recirculation, as is evidenced by the large negative skin friction values. The reattachment point, where skin friction becomes positive, is close to the experimental value. Beyond the reattachment point the skin friction recovers slower than the experimental measurements. This solution mimics the reference Spalart-Allmaras solution posted on the NASA Langley Turbulence Modeling Resource website.[6]

The LES solutions employ the SEM inflow boundary condition and start much closer to the step. For grid 1, the SEM boundary was placed at $x/H = -8$. The C_f drops quickly downstream of the inflow and never recovers to the desired value before reaching the step. It was assumed that the grid resolution was not sufficient to properly sustain the turbulent boundary layer. Grid 2 used the same inflow plane position, but has more resolution. For this case, the skin friction drops downstream of the inflow plane, but then recovers to the correct value. This behavior is typical of the SEM method. The turbulent flowfield created by the SEM is an approximation and does not satisfy the flow solver's numerical representation of the Navier-Stokes equations. Immediately downstream of the inflow plane the solver forces the flow to satisfy the equations. This causes the flow to no longer match the specified inflow boundary conditions. These

two competing processes create a region where the flow eventually adjusts to both satisfy the equations and match the desired inflow conditions. Grid 3 uses the same upstream resolution, but moves the inflow plane to $x/H = -12$ to allow more time and distance for the flowfield to adjust and develop.

Downstream of the step, the coarsest grid LES solution predicts a narrower and stronger recirculating region, with the flow reattaching too far upstream. The refined grid 2 result, shows a much better prediction of the skin friction in the recirculating zone and reattachment point. Both grids 1 and 2, begin to stretch at $x/H = 12$ and results beyond this point are not reliable. Grid 3, has the finest resolution in the recirculating zone. Its prediction of the skin friction is very similar to grid 2, but the flow reattaches somewhat sooner. This grid begins to stretch at $x/H = 15$ and thus the skin friction prediction in the aft portion of the plot is improved. The reattachment point is often used as a figure of merit in studies such as these and the present results are given in table 4. It must be noted that the reattachment point can be significantly affected by the assumptions made with regard to two-dimensionality of the flow. While care was taken in the experiment to generate a two-dimensional flow, sidewall affects and some three-dimensionality can not be completely ignored. The use of a $4H$ wide domain and periodic span-wise boundary conditions for the LES, is an assumption that needs further examination. Ideally a full three-dimensional simulation should be undertaken, but would be much more costly. In lieu of a full 3D study, sensitivity to the quasi-2D domain width should be examined.

Table 4: Reattachment location

	x/H
Expt.	6.26 ± 0.10
RANS	6.30
LES Grid 1	4.91
LES Grid 2	6.20
LES Grid 3	6.03

C. Reference Station Predictions

Mean velocity and Reynolds stresses at the reference station, $x/H = -4$, are shown in figure 6. The mean velocity for all solutions matches well with the experiment (figure 6a). The largest differences appear to occur in the logarithmic region. For the Reynolds normal stresses (figures 6b & 6c), the coarsest grid LES provides a good prediction of the axial component, but under-predicts the vertical component. This is typical of an under-resolved LES. The finer grid LES solutions (grid 2 & 3) both over-predict all of the stresses. The grid 3 solution is closer to the experiment for all components, indicating that the longer boundary layer development length between the SEM inflow plane and this station is beneficial. Recall that the grid resolution in the upstream section for both grids 2 and 3 is identical. Therefore both a longer boundary layer development length, or finer grids may be necessary to improve the comparison with the experiment. The RANS solution under-predicts the axial normal stress and over predicts the vertical normal stress. It does the best job at predicting the shear stress. This is not surprising as RANS turbulence models do a very good job predicting zero pressure gradient turbulent boundary layers. As noted earlier only the shear component of the Reynolds stress is used in the RANS equations; the normal stresses are approximated here for comparison, but they are not relevant for the solution.

D. Separation Zone Predictions

Velocity profiles, Reynolds stresses and triple product velocity correlations will be compared in the separated region at $x/H = 1, 4, 6,$ and 10. Time-averaged velocity profiles are shown in figure 7. The grid 1 LES predicts the smallest and weakest separation, as evidenced by the lowest reverse axial velocities and largest downward velocities. This fact is corroborated by the reattachment location data presented previously. The RANS solution is an outlier at $x/H = 1.0$, showing much larger velocity magnitudes at this location. The LES solutions on grids 2 & 3 are similar, with only slight differences due to the increased resolution of grid 3 in this region. All methods under-predict the magnitude of the downward velocity in the downstream profiles

(x/H = 6 and 10). The reason for this is unclear, but likely indicates that all methods have incorrectly predicted the details of the separation strength and/or size.

Reynolds stresses are shown in figure 8. The RANS solution under-predicts the stresses near the wall ($y/H < 0.5$). This is most pronounced in the axial normal stress, but is true for components. For the LES solutions, the coarse grid yields overly large values of for all stresses. This is typical of under-resolved LES solutions; the lack of resolution forces the turbulent energy into the largest scales. The finer grid LES solutions are again very similar, indicating that the solution on grid 3, may be close to grid convergence. The differences between grid 2 and 3 could also be attributed to the differences in the upstream boundary layer development, as the differences in the flows at the reference station were significant. This warrants further study.

Triple product velocity correlations, $< u_i u_j u_k >$, represent the turbulent transport of the Reynolds stresses. These quantities are not often measured in validation experiments, especially one performed in the 1980's. This data provides an opportunity to assess LES's ability to compute these terms and to determine if additional resolution is required over that needed for the mean flow and Reynolds stress data. This data cannot be extracted from a RANS solution. Data for the three LES solutions is shown in figure 9. The data for all four quantities, $< uuu >$, $< vvv >$, $< uvv >$, and $< vuu >$, exhibit an "S-shaped" curve, centered about the zero axis. All three LES solutions predict the correct shapes. However, the position of the top inflection point is consistently higher than the experimental data. As with the other results, the grid 1 solution displays higher magnitudes due to its lack of resolution. There are slight differences between grids 2 and 3, with the finer grid, slightly closer to the data. Additional grid refinement should be explored to see if it improves these predictions.

Overall the grid 3 LES solution is a reasonable replication of the experimental flow field. However as mentioned previously, some additional work should be undertaken before more detailed analyses, such as investigating turbulence budgets and RANS model terms is performed.

V. Summary and Conclusions

Numerical simulations of the subsonic flow over a backward facing step were performed to examine and improve the capability to predict reattaching flows. A Reynolds-averaged Navier-Stokes simulation using the Spalart-Allmaras turbulence model and three large-eddy simulations on grids of increasing resolution were performed. All simulations were done using the high-order of accuracy finite-difference solver, WRLES. The results were compared to the experimental data of Driver and Seegmiller.[4] The experiment was carried out in a high-aspect ratio facility to provide as two-dimensional a flow as possible. The simulations assume two-dimensional flow. For this case the RANS simulation provides reasonable agreement with the data and it provided detailed flow conditions upstream of the step for the LES's turbulent inflow boundary condition, and initial conditions.

The LES utilized the synthetic eddy method in order to minimize the amount of grid upstream of the step. Modifying the SEM to include fluctuations to density and temperature reduced pressure fluctuations at the inflow and improved stability. It was found that the coarsest grid LES did not provide enough resolution to accurately reproduce the upstream turbulent boundary layer. A finer grid correctly predicted the skin friction upstream of the step. It was also determined that the distance between the SEM inflow plane and the reference plane was important. While the initial distance of 8 step heights was sufficient to achieve the correct skin friction at the reference plane, a longer distance of 12 step heights showed improved predictions of the Reynolds stresses at the same plane. Further work to examine an even longer distances is recommended.

In the separated region downstream of the step, the LES simulations did a reasonable job predicting the mean flow, Reynolds stresses and triple product velocity correlations. The coarse grid results significantly over-predicted the magnitudes of the Reynolds stresses and triple products. The two finer grids, provided very similar data much closer to the experimental values. However, there is still room for improvement and there are several recommendations for future work. First, finer grids both upstream and downstream of the step should be explored to achieve grid converged solutions. Ideally this should be done separately to study the effect of the upstream resolution on the separation prediction. Next, the quasi-2D assumption should be explored. This investigation should include simulations of both increased- and decreased-width periodic domains, along with a full three-dimensional case with sidewall boundary layers, if resources allow. Ultimately, more in depth flowfield analyses should be done including documenting the time-dependent behavior of the separation and obtaining turbulence budgets.

Acknowledgements

This research was sponsored by NASA's Transformational Tools and Technologies (TTT) Project of the Transformative Aeronautics Concepts Program under the Aeronautics Research Mission Directorate. Resources supporting this work were provided by the NASA High-End Computing (HEC) Program through the NASA Advanced Supercomputing (NAS) Division at Ames Research Center.

References

[1]Slotnick, J., Khodadoust, A., Alonso, J., Darmofal, D., Gropp, W., Lurie, E., and Mavriplis, D., "CFD Vision 2030 Study: A Path to Revolutionary Computational Aerosciences," NASA CR 2014-218178, 2014.

[2]Spalart, P. R. and Allmaras, S. R., "A One-Equation Turbulence Model for Aerodynamic Flows," AIAA Paper 92-0439, 1992.

[3]Menter, F. R., "Two-Equation Eddy-Viscosity Turbulence Models for Engineering Applications," *AIAA Journal*, Vol. 32, No. 8, 1994, pp. 1598–1605.

[4]Driver, D. and Seegmiller, H., "Features of a Reattaching Turbulent Shear Layer in Divergent Channel Flow," *AIAA Journal*, Vol. 23, No. 2, 1985, pp. 163–171.

[5]DeBonis, J., "WRLES: Wave Resolving Large-Eddy Simulation Code, Theory and Usage," NASA TM 2019-220192, 2019.

[6]C. Rumsey, "Langley Turbulence Modelin Resource," http://www.turbmodels.larc.nasa.gov, 2020, [Online; accessed 29-October-2020].

[7]J.W. Slater, "NPARC Alliance Verification and Validation Archive," https://www.grc.nasa.gov/WWW/wind/valid/archive.html, 2015, [Online; accessed 29-October-2020].

[8]"European Research Community on Flow Turbulence and Combustion, Classic Collection Database," http://cfd.mace.manchester.ac.uk/ercoftac/doku.php, 2020, [Online; accessed 29-October-2020].

[9]Forum, M. P. I., *MPI: A Message-Passing Interface Standard, Version 2.2* , High Performance Computing Center Stuttgart (HLRS), 2009.

[10]Chapman, B., Jost, G., and van der Pas, R., *Using OpenMP: Portable Shared Memory Parallel Programming*, The MIT Press, 2007.

[11]DeBonis, J. R. and Scott, J. N., "A Large-Eddy Simulation of a Turbulent Compressible Round Jet," *AIAA Journal*, Vol. 40, No. 5, 2002, pp. 1346–1354.

[12]DeBonis, J. R., "An Examination of the Spatial Resolution Requirements for LES of a Compressible Jet," *Quality and Reliability of Large-Eddy Simulation II*, edited by M. V. Salvetti, B. Geurts, H. Meyers, and P. Sagaut, Springer, 2010, pp. 329–338.

[13]DeBonis, J. R., "A High-Resolution Capability for Large-Eddy Simulation of Jet Flows," AIAA Paper 2010-5023, 2010.

[14]DeBonis, J., "Solutions of the Taylor-Green Vortex Problem Using High-Resolution Explicit Finite Difference Methods," AIAA Paper 2013-0382, 2013.

[15]DeBonis, J. R., "Prediction of Turbulent Temperature Fluctuations in Hot Jets," *AIAA Journal*, Vol. 56, No. 8, 2018, pp. 3097–3111.

[16]Bogey, C. and Bailly, C., "A Family of Low Dispersive and Low Dissipative Explicit Schemes for Flow and Noise Computations," *Journal of Computational Physics*, Vol. 194, 2004, pp. 194–214.

[17]Tam, C. K. W. and Shen, H., "Direct Computation of Nonlinear Acoustic Pulses Using High Order Finite Difference Schemes," AIAA Paper 93-4325, 1993.

[18]Kennedy, C. A. and Carpenter, M. H., "Comparison of Several Numerical Methods for Simulation of Compressible Shear Layers," NASA TP 3484, 1997.

[19]Berland, J., Bogey, C., Marsden, O., and Bailly, C., "High-Order, Low Dispersive and Low Dissipative Explicit Schemes for Multiple-Scale and Boundary Problems," *Journal of Computational Physics*, Vol. 224, 2007, pp. 637–662.

[20]Berland, J., Bogey, C., and Bailly, C., "Low-Dissipation and Low-Dispersion Fourth-Order Runge-Kutta Algorithm," *Computers and Fluids*, Vol. 35, 2006, pp. 1459–1463.

[21]Jarrin, N., Benhamadouche, S., Laurence, D., and Prosser, R., "A Synthetic-Eddy-Method for Generating Inflow Conditions for Large-Eddy Simulations," *International Journal of Heat and Fluid Flow*, Vol. 27, No. 4, 2006, pp. 585–593.

[22]Touber, E. and Sandham, N., "Oblique Shock Impinging on a Turbulent Boundary Layer: Low-Frequency Mechanisms," AIAA Paper 2008-4170, 2008.

[23]Georgiadis, N. J., Rumsey, C. L., Yoder, D. A., and Zaman, K. B. M. Q., "Turbulence Modeling Effects on Calculation of Lobed Nozzle Flowfields," *Journal of Propulsion and Power*, Vol. 22, No. 3, 2006, pp. 567–575.

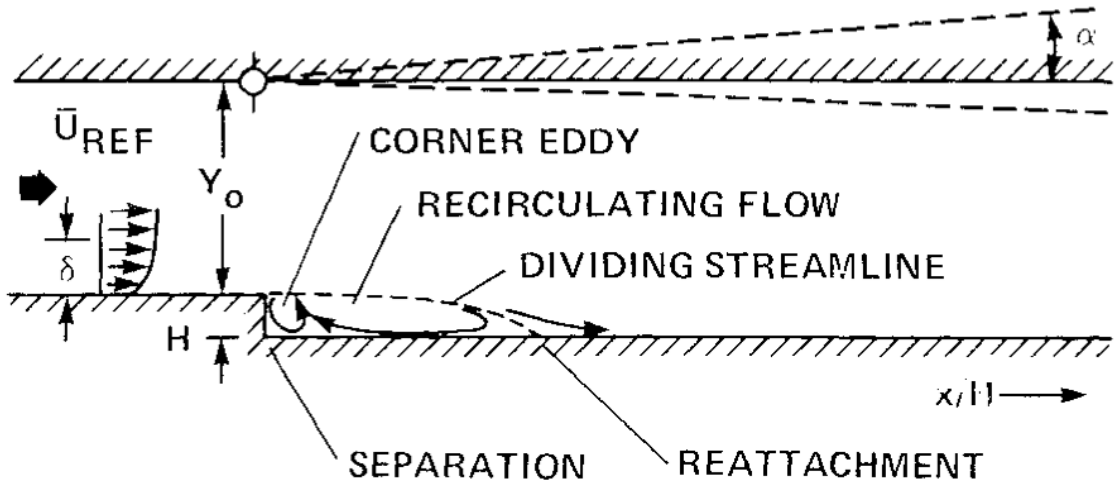

Figure 1: Schematic of flowfield and experimental test rig

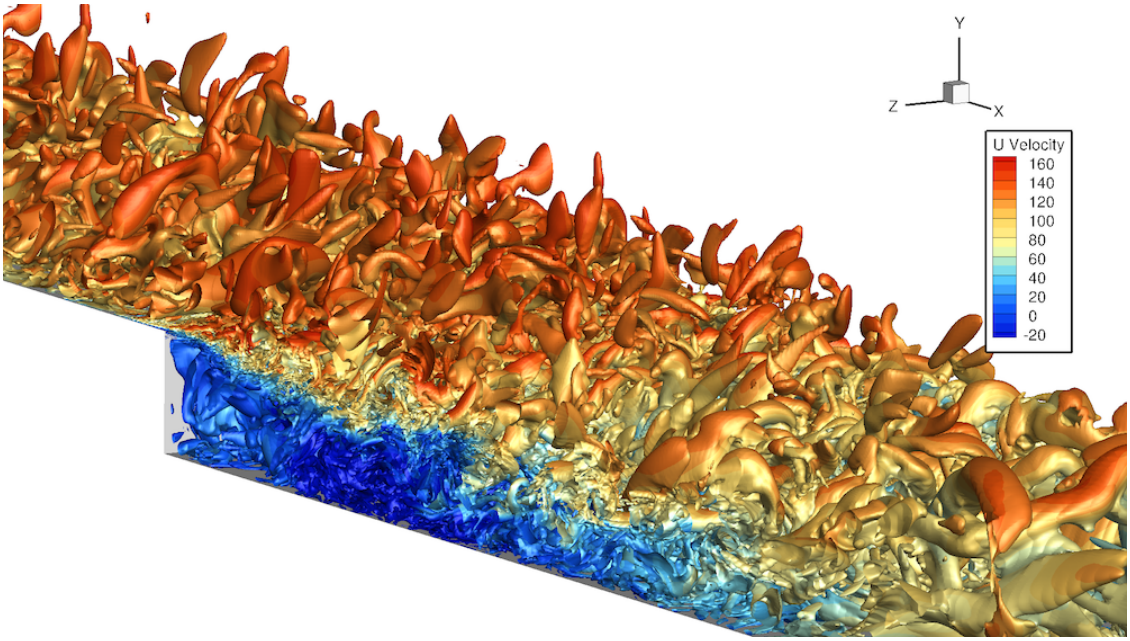

Figure 2: Iso-surfaces of q-criterion colored by axial velocity

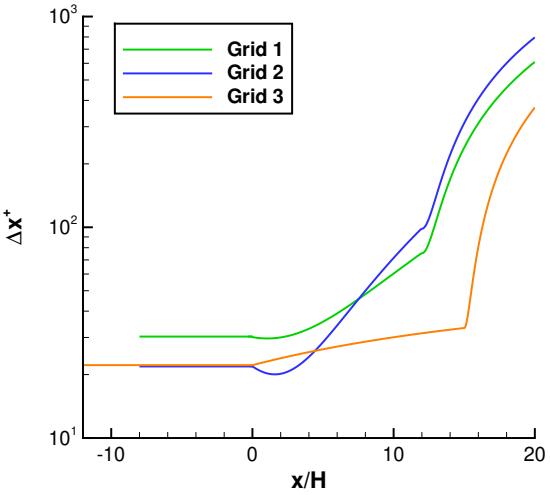

(a) x^+-spacing

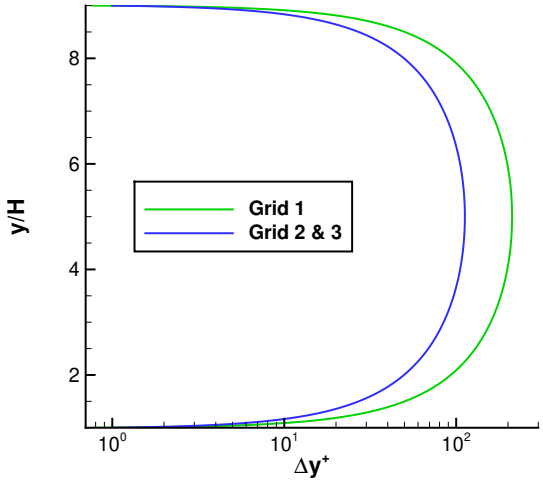

(b) y^+-spacing, ref. plane, $x/H = -4$

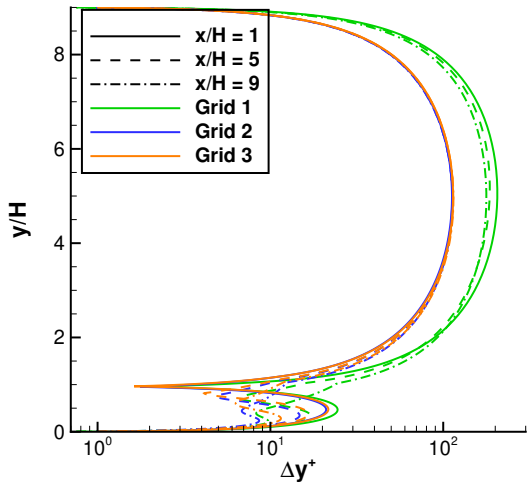

(c) y^+-spacing, $x/H = 1, 5$ & 9, $0 \leq y/H \leq 9$

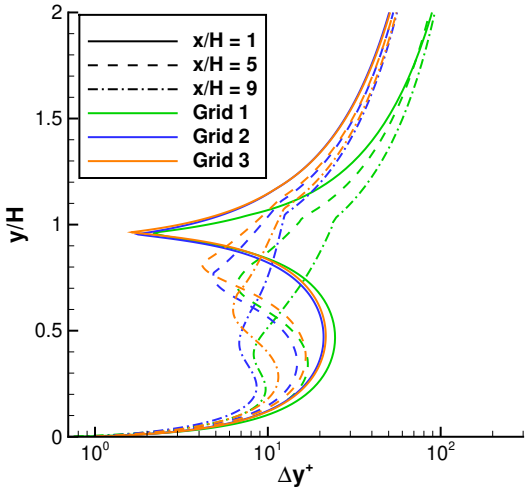

(d) y^+-spacing, $x/H = 1, 5$ & 9, $0 \leq y/H \leq 2$

Figure 3: Grid spacings for the LES grids

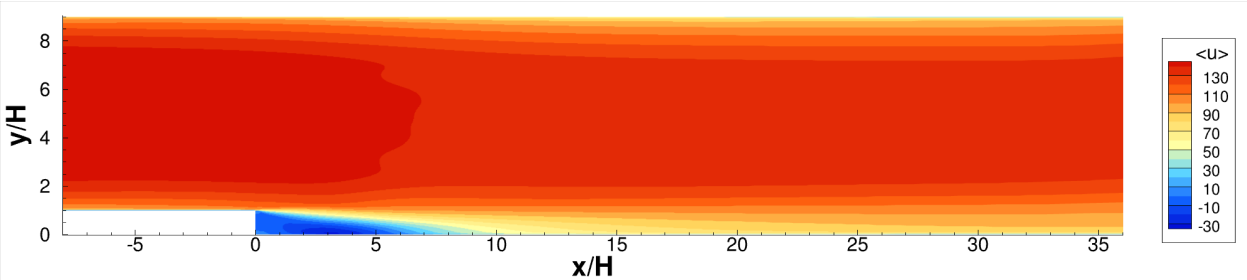

(a) $-8 < x/H < 36$

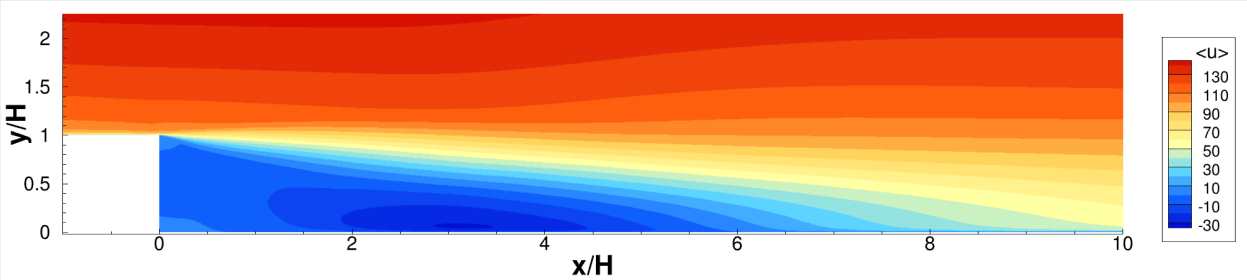

(b) $-1 < x/H < 10$

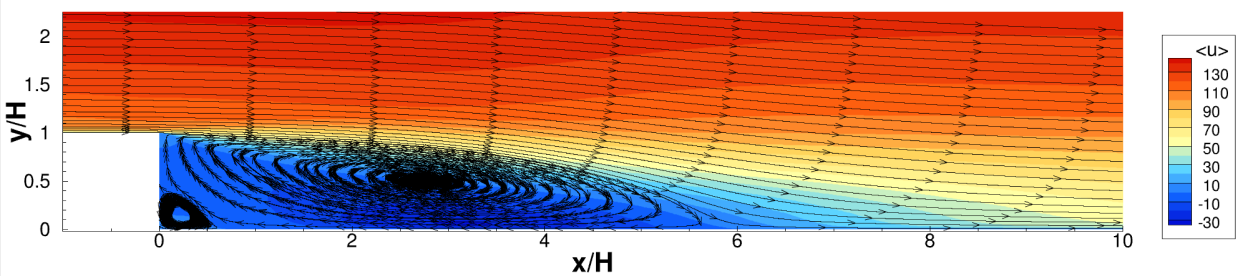

(c) $-1 < x/H < 10$, with streamlines

Figure 4: Time averaged axial velocity contours, $< u >$, from the LES solution on the finest grid (grid 3)

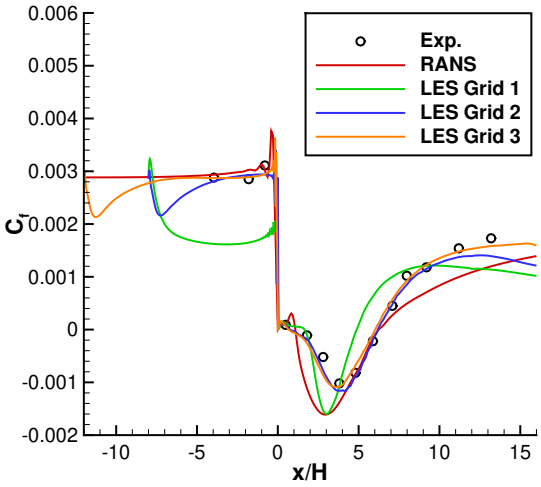

Figure 5: Skin friction coefficient

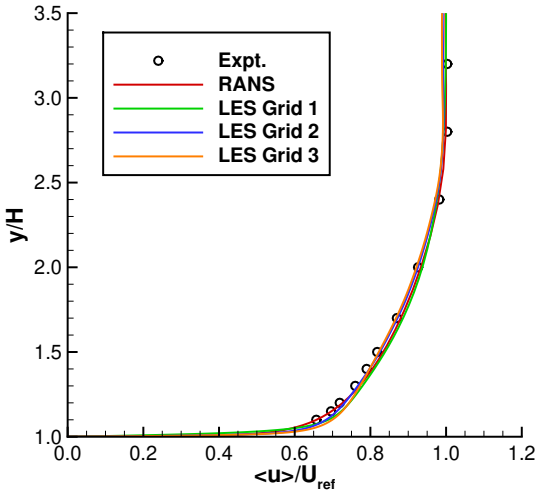

(a) axial velocity, u/U_{ref}

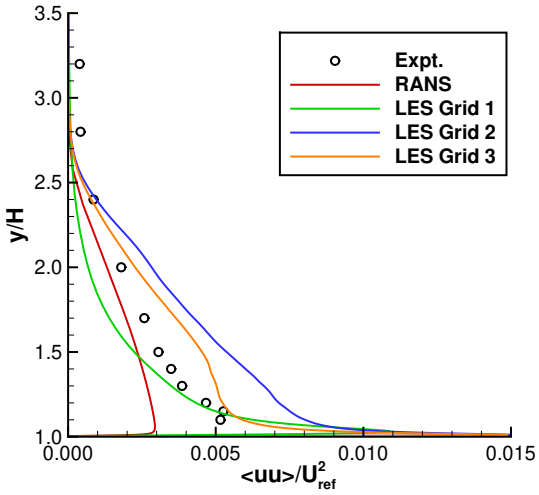

(b) Axial normal stress, $< uu > /Uref^2$

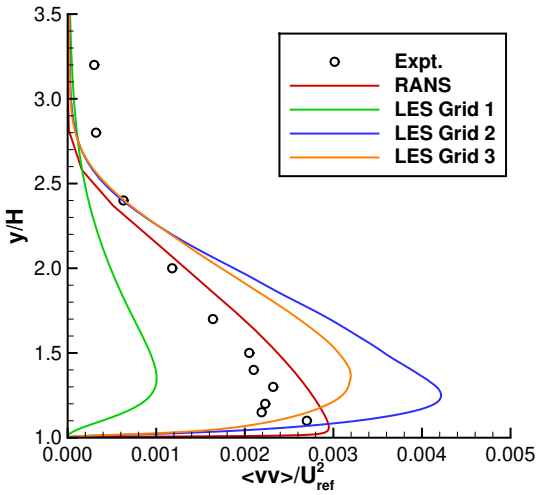

(c) Vertical normal stress, $< vv > /Uref^2$

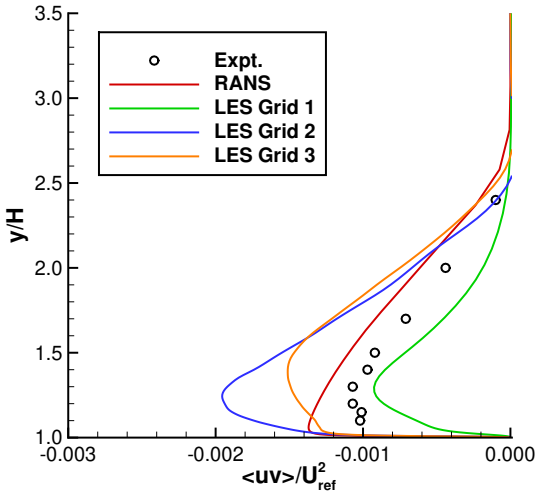

(d) Shear stress, $< uv > /Uref^2$

Figure 6: Reference station, $x/H = -4$, flow profiles

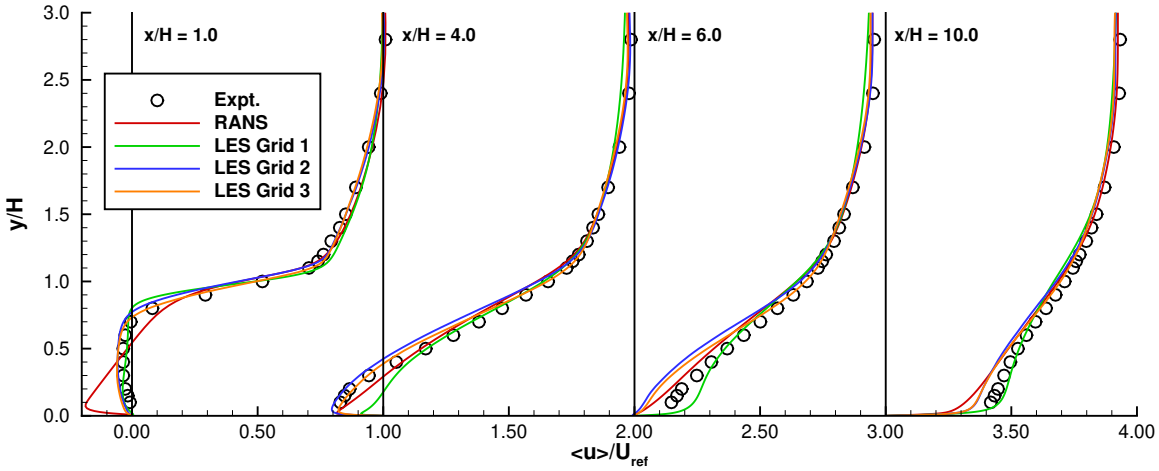

(a) axial velocity, $< u > /U_{ref}$, subsequent profiles shifted 1.0

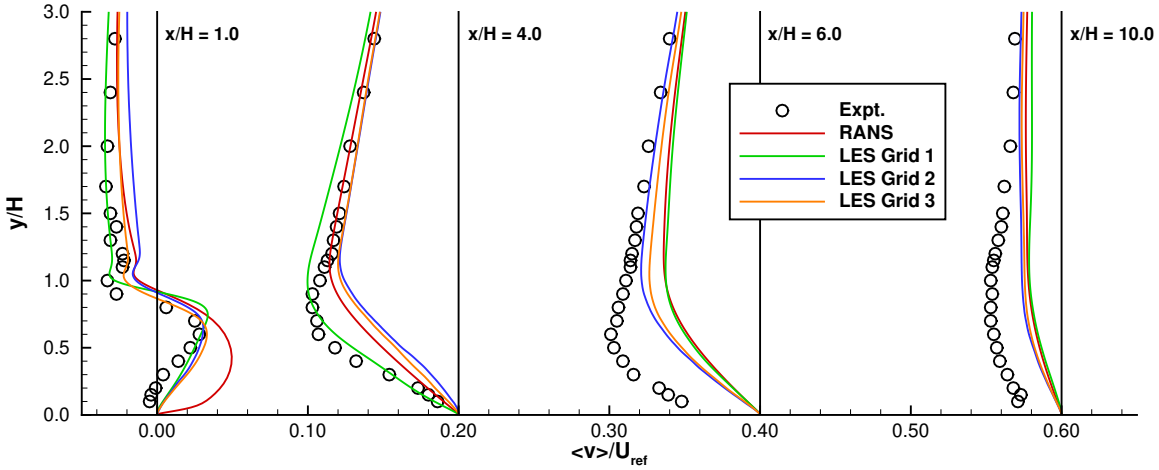

(b) vertical velocity, $< v > /U_{ref}$, subsequent profiles shifted 0.2

Figure 7: Velocity profiles downstream of the step

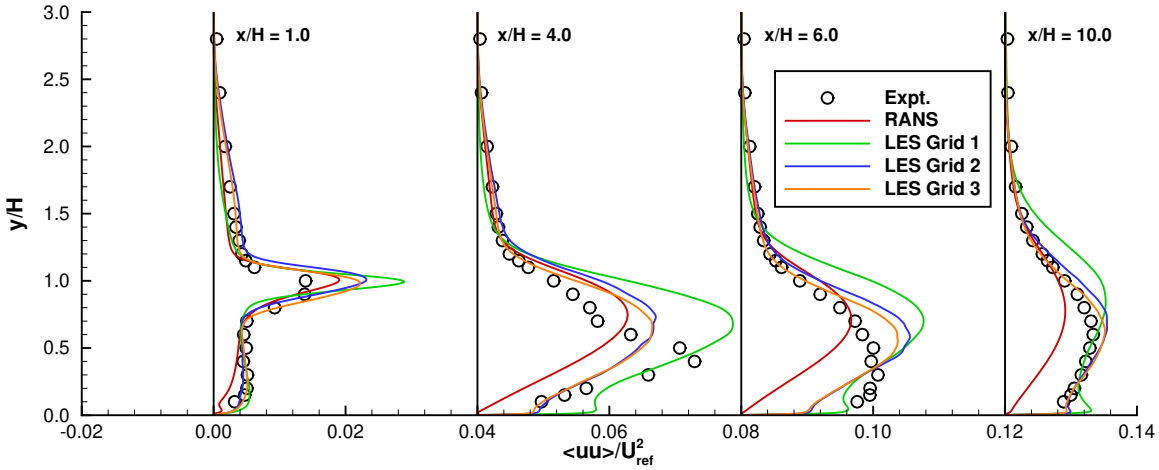

(a) Axial normal stress, $< uu > /U^2_{ref}$

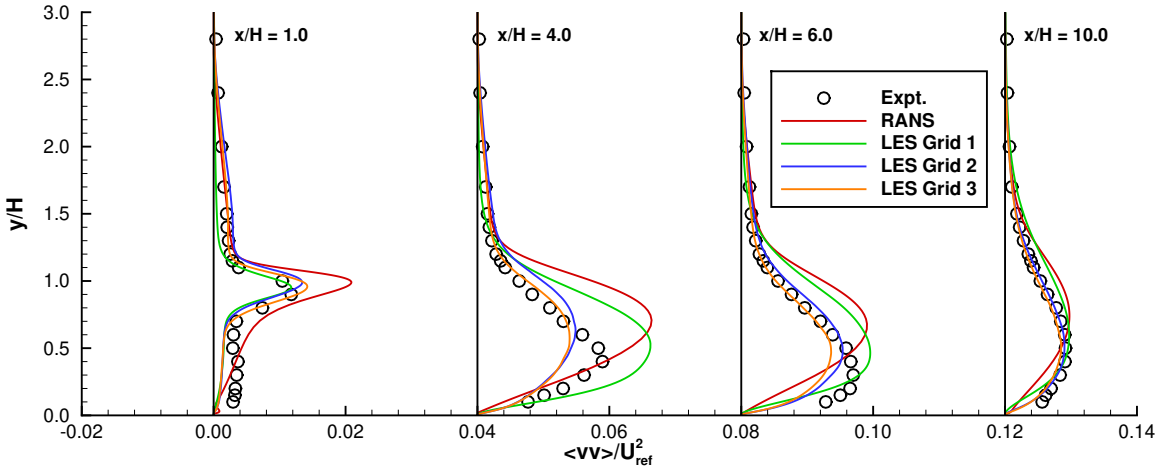

(b) Vertical normal stress, $< vv > /U^2_{ref}$

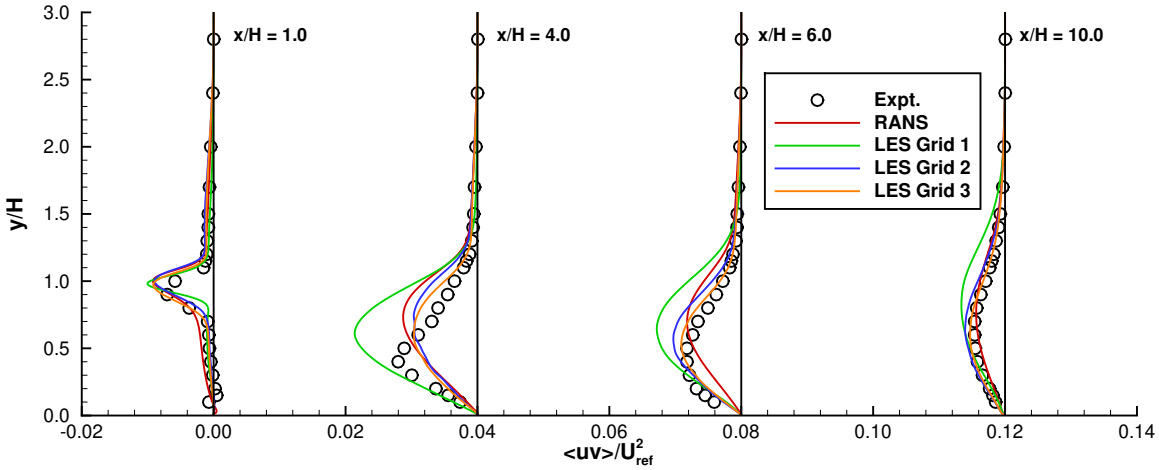

(c) Shear stress, $< uv > /U^2_{ref}$

Figure 8: Reynolds stress profiles downstream of the step, subsequent profiles shifted 0.04

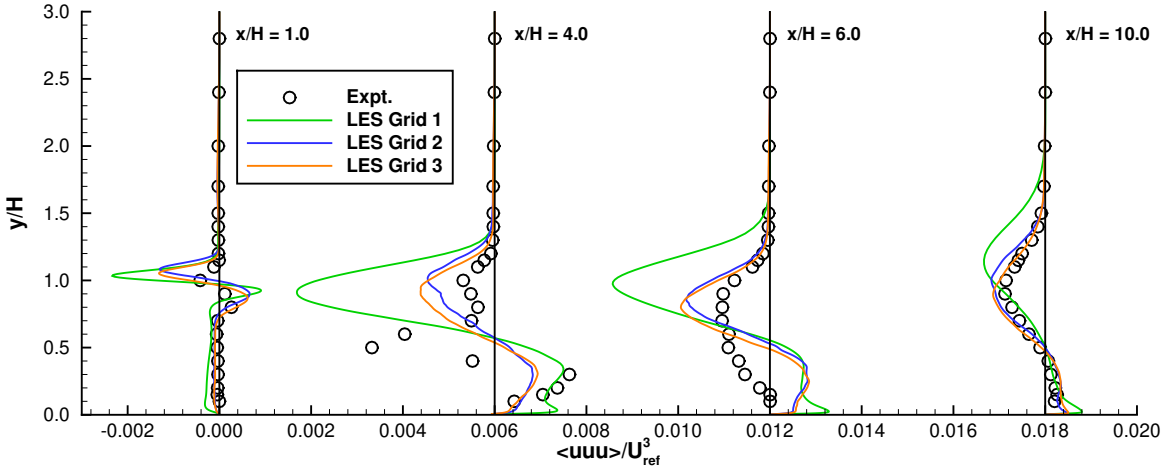

(a) $< uuu > /U^3_{ref}$

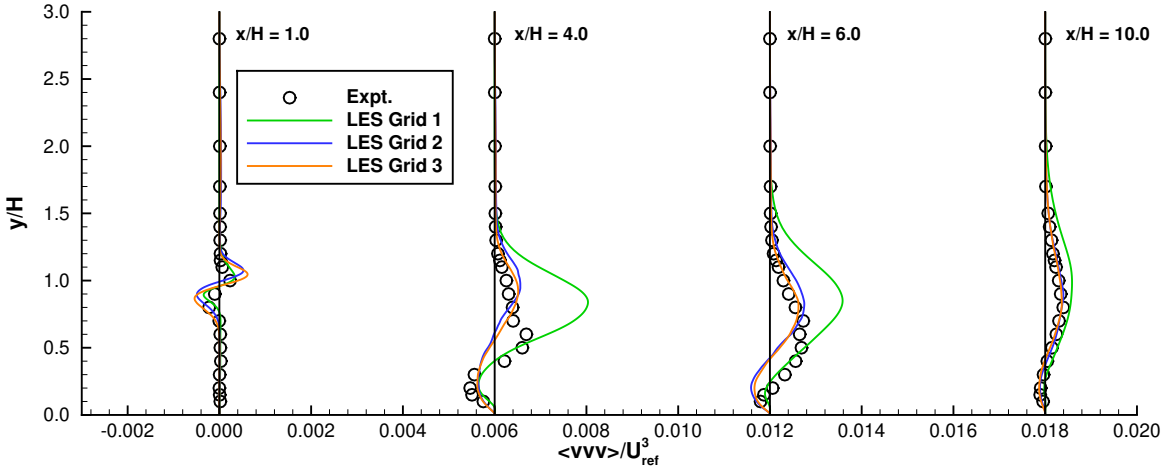

(b) $< vvv > /U^3_{ref}$

Figure 9: Triple product profiles downstream of the step, subsequent profiles shifted by 0.006

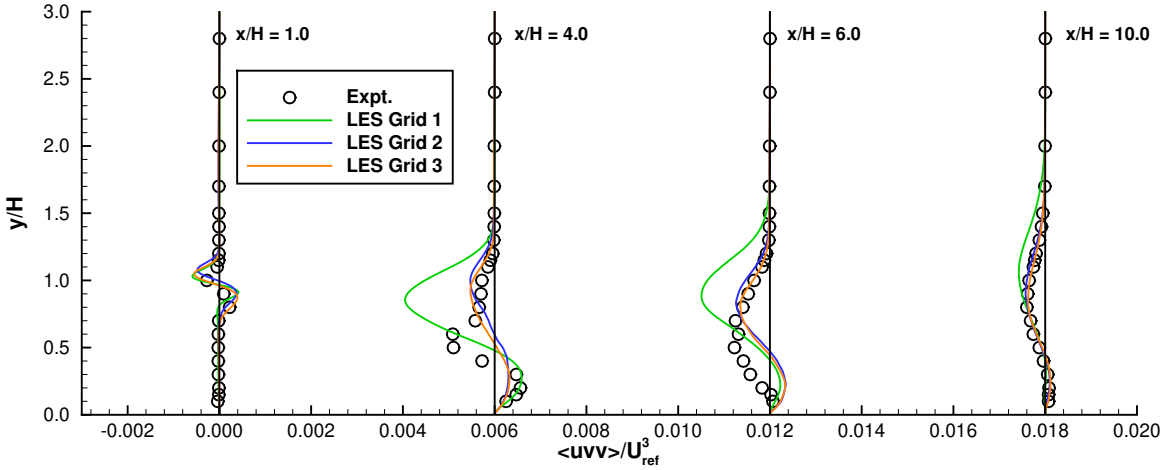

(c) $< uvv > /U^3_{ref}$

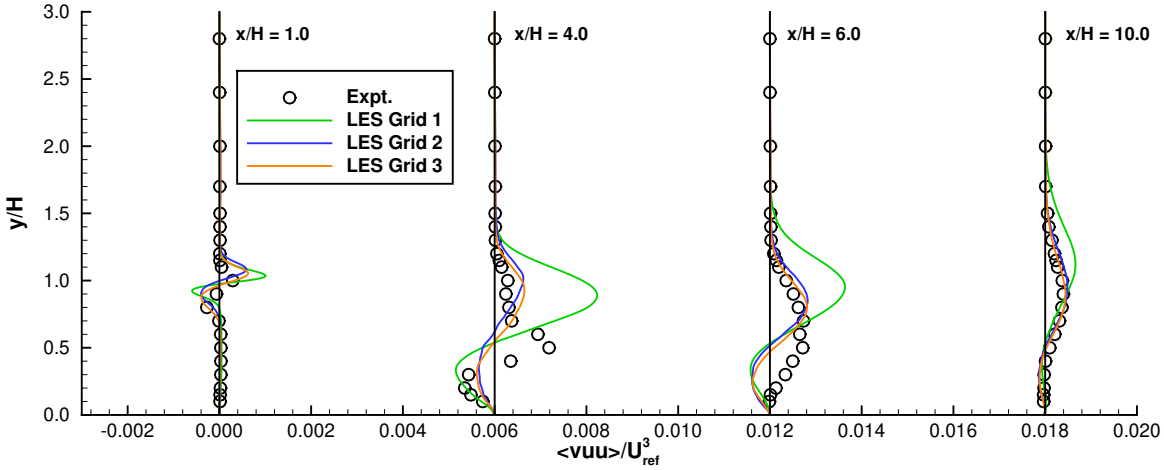

(d) $< vuu > /U^3_{ref}$

Figure 9: Triple product profiles downstream of the step, subsequent profiles shifted by 0.006, [continued]